University of Texas at El Paso
DigitalCommons@UTEP

Open Access Theses & Dissertations

2009-01-01

Detection of Gas/Odor Based on Quartz Crystal Microbalance Sensors and Fuzzy Similarity Measure

Yi-Chen Lo
University of Texas at El Paso, yichenlo@gmail.com

Follow this and additional works at: https://digitalcommons.utep.edu/open_etd

 Part of the Electrical and Electronics Commons

Recommended Citation
Lo, Yi-Chen, "Detection of Gas/Odor Based on Quartz Crystal Microbalance Sensors and Fuzzy Similarity Measure" (2009). *Open Access Theses & Dissertations*. 302.
https://digitalcommons.utep.edu/open_etd/302

This is brought to you for free and open access by DigitalCommons@UTEP. It has been accepted for inclusion in Open Access Theses & Dissertations by an authorized administrator of DigitalCommons@UTEP. For more information, please contact lweber@utep.edu.

DETECTION OF GAS/ODOR BASED ON QUARTZ CRYSTAL MICROBALANCE SENSORS AND FUZZY SIMILARITY MEASURE

YI-CHEN LO

DEPARTMENT OF ELECTRICAL AND COMPUTER ENGINEERING

APPROVED:

_____
Thompson Sarkodie-Gyan, Ph.D., Chair

_____
David Zubia, Ph.D

_____
Patricia Nava, Ph.D.

_____
Tzu-Liang (Bill) Tseng, Ph.D.

_____
Patricia D. Witherspoon, Ph.D.
Dean of the Graduate School

The thesis is dedicated

to my parents, Ko-Lung Lo and Fang-Wei Tseng

my lovely girlfriend, Ning Hsu

and my beautiful family

DETECTION OF GAS/ODOR BASED ON QUARTZ CRYSTAL MICROBALANCE SENSORS AND FUZZY SIMILARITY MEASURE

YI-CHEN LO

THESIS

Presented to the Faculty of the Graduate School of

The University of Texas at El Paso

in Partial Fulfillment

of the Requirements

for the Degree of

MASTER OF SCIENCE

DEPARTMENT OF ELECTRICAL ENGINEERING

THE UNIVERSITY OF TEXAS AT EL PASO

December 2008

ACKNOWLEDGMENTS

First of all, I would like to thank my parents and my family for encouraging me to pursue a higher education and supporting me part of the expense during my studying. I also would like to thank my girlfriend, Ning Hsu, for helping me with my livelihood. Because of them, I can concentrate on my studies and accomplish my degree of Master of Science.

I want to thank my kindly adviser, Dr. Thompson Sarkodie-Gyan, who is both a wonderful mentor and a good friend. His professional guidance and providence strengthen my ability of individual research and capacity of dealing with complicated tasks. I want to thank Dr. David Zubia for the utilization of nanomaterials integration laboratory and members of this laboratory. Their helps facilitate preparations and processes of experiment.

I wish to thank Sandia National Laboratory for the cooperation of coating QCM sensors, Oxazogen Inc. for the donation of BSP3 polymer, and Ohio Valley Specialty Company for the donation of OV-275 polymer.

Moreover, I want to thank Dr. Wen-Yee Lee and Dr. Michael Eastman for the counseling of polymer coating, friends in chemistry department and biological science department for the help of polymer coating and David Powell for the help of fabricating the experimental structure.

Finally, I would like to extend my thanks to all my friends in the Laboratory of Industrial Metrology and Automation for giving me some beneficial suggestions and Dr. Patricia Nava and Dr. Tzu-Liang (Bill) Tseng for kindly being on my thesis committee.

ABSTRACT

In this research, an array of six Quartz Crystal Microbalance sensors (QCM) using fuzzy similar measurement is proposed to recognize different gases and the percentage of those gases in a mixed gas. The experiment suggests three different gases, oxygen, helium, and argon as test gases and the nitrogen as the reference gas. Six QCMs in this array are coated respectively with six different specific polymers that are selected based on Linear Solvation Energy Relationship (LSER) method, in order to absorb gas molecules so as to recognize responses of resonant frequency changes from QCMs. Testing with different gases results in different responding patterns from QCMs array, which means the possibility of differentiating a gas from the others by comparing the responding pattern of the gas with other patterns, e.g. the pattern of oxygen is different from the pattern of helium and argon. Based on the pattern recognition, an idea of perceiving a correct percentage of a specific gas in a mixed gas is also introduced; this idea is realized by comparing response patterns with a diversity of percentage of the same gas. Fuzzy similarity comparison provides an alternative way to deal with the issue of pattern recognition. The most crucial part of fuzzy similarity comparison is to establish a database of response patterns which is able to recognize not only the type of the gas detected, but also the percentage of the gas in the air.

TABLE OF CONTENTS

Page

LIST OF TABLES

Page

LIST OF FIGURES

Page

CHAPTER 1

INTRODUCTION

The development of biosensors has become a novel and innovative research area to the highly developed society; the similar characteristics of each biosensor is to perform a function of detecting a property of analytes and then transferring it to an electronic signal for the purpose of measuring and analyzing. Currently, the electronic nose (e-nose) based on gravimetric sensors, for example, is one of the biosensors which have been proposed to mimic mammalian olfactory system. The application of electronic nose involves detections of a wide variety of odorant and volatile organic components (VOCs), such as in the food industry, real-time volatile gases monitoring, and in medical diagnosis, etc.

1.1 Olfactory System

1.1.1 Biological Olfactory System

The biological olfactory system provides an ability to distinguish among different flavors by sensing a variety of molecules of them. The reason why this system is able to perform this discrimination is due to three important components, a variety of chemical sensors called the olfactory receptors, the olfactory bulb which performs signal processing and the olfactory cortex which is an odor recognition system in the brain. The process of olfactory has the following steps: First, it begins with sniffing which brings odorous molecules from free air into the olfactory system and also mixes them into a uniform concentration. Second, these molecules from free air dissolve in a thin mucus layer which acts as a filter to remove larger particles and transports odorous molecules to the olfactory receptor neurons. Third, once the molecules chemically stimulate the receptors, the reaction between molecules and receptor produces signals that are

sent by the axon from receptors to the olfactory bulb which is located in the brain. The signals continue into the olfactory bulb to the olfactory cortex which is located in the brain, and this is able to perform odor recognition [1]. Figure 1-1 illustrates the main components of the olfactory system.

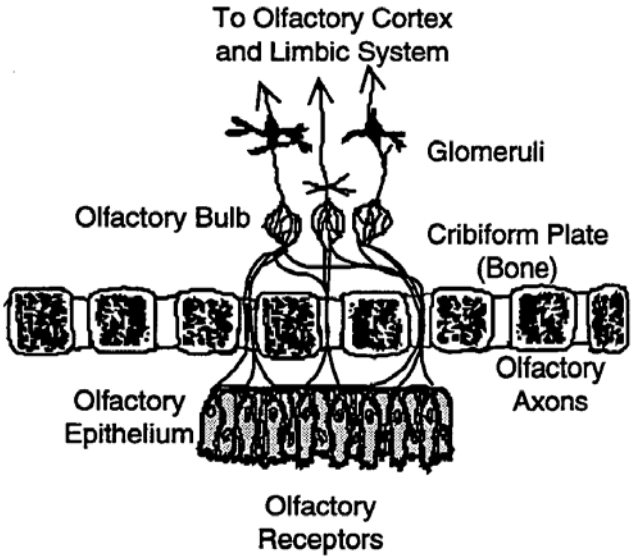

Figure 1-1. The figure of three main components of the olfactory system: olfactory sensors, olfactory bulb and olfactory cortex.

1.1.2 The Sensing of Odorant

In mammalian olfactory system, the secret of how the olfactory system perceives odorant was discovered by Richard Axel and Linda B. Buck, the winners of 2004 Nobel Prize in Physiology/Medicine, and is considered as a great discovery on human sensing system. They found that around 1000 gens in mice give rise to an equivalent number of types of olfactory receptor, and 350 types in human. The diversity of olfactory receptor cells is responsible for odorous detections and each cell contains only one type of receptor. They also found that the perception of an odorant is basically derived from a specific number of receptors and a specific

combination of receptors that are activated for a certain level. Accordingly, the discovery clearly proves that any pattern of the receptor signal represents a fingerprint of an odorant and is a crucial key for mammalian to be able to smell thousands of flavors [2, 3, 4].

1.2 Electronic Nose

Since biological noses have limitations in a variety of odors and vapors due to sensitivity and toxic issues on them, alternative ways to replace biological noses for discriminating odorants and vapors are becoming an essential topic in a variety of industries, such as food, drink, perfumery, and environmental monitoring, etc. Therefore, an artificial gas detector or Electronic Nose is proposed to mimic biological noses. Basically, the electronic Nose is one of the biosensors performing similar characteristics to the biological olfactory system. Like an olfactory system, it mainly consists of two separated systems, a sensing system and a recognition system. The sensing system includes a set of chemical sensors that sense odorants and turn out responses. By providing those responses of the sensor system to the recognition system, the fingerprints of detected odorants can be found based on the different characteristics of them. In the literature, different kinds of mass variation sensors, for example, quartz crystal microbalance (QCMs), surface acoustic wave sensor (SAWs), and bulk acoustic wave sensor (BAWs), are able to perform similar functionalities that can be applied to electronic nose [5]. Comparing electronic the nose with the olfactory system, the sensor system represents the receptors that are able to extract signals and send them to the recognition system, the brain. The following table manifestly displays an important comparison of the similar functionalities between an olfactory system and the electronic nose system.

Table 1-1. Comparison of Human Olfactory System and Electronic System.

	Sensing System	Pattern Recognition
Human Olfactory System	Receptors	Brain
Electronic Nose System	QCM Sensors	Database

1.3 Acoustic Wave Sensors

According to different types of needs, there are a variety of acoustic wave sensors developed for the applications of chemical sensing in both gas and liquid phases. Those acoustic wave sensors widely incorporate thickness shear mode (TSM) devices, surface acoustic wave (SAW) devices, leaky SAW devices, surface transverse wave (STW) device, love wave devices, shear-horizontal acoustic plate mode (SH-APM) devices, flexural plate wave (FPW) devices, thin film resonators, and thin rod flexural devices [6]. In gas phase application, the important characteristic of the acoustic wave devices is the sorption step where the reactions between sorbent film deposited on devices and analytes take place, and the measurable features are able to change via the process of sorption. The sorption process involves two types, the adsorption which alters the measurable features while analytes deposit onto the sorbent film, and the absorption which alters the measurable features while analytes go into the bulk of the sorbent film. From figure 1-2, the sorption process of the vapor molecules from gas phase to the sorbent film is clearly illustrated [7]. The vapor in the air changes the measurable features (mass of the film) by either being absorbed into or adsorbed onto the film.

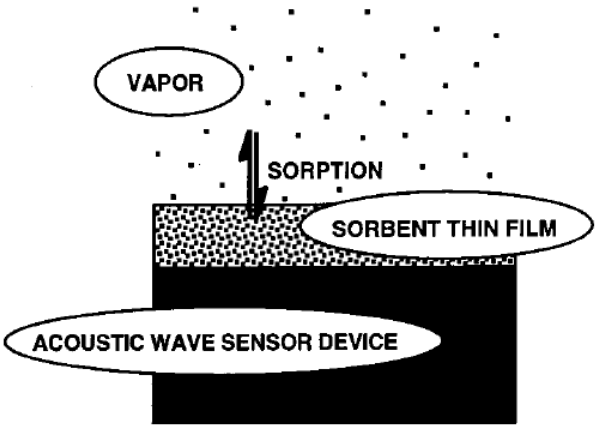

Figure 1-2. The schematic diagram of the sorption of vapor molecules.

Generally, two different types of acoustic wave sensors are commonly used in the gas detection, TSM and SAW, and their schematic figures of top view and side view are shown in the figures 1-3 [7]. In this discussion, the spotlight is mainly focused on the TSM device in the gas-phase application and the details will be discussed in the later sections. TSM device, also called bulk acoustic wave (BAW) device or quartz crystal microbalance (QCM), is widely utilized in a lot of research tasks because of its availability, robust nature, low cost, affordable electronics, and the physical property of being sensitive to very small mass attaching on the surface of it, even though FPW and SAW are still considered more sensitive than QCM [8]. The quartz crystal microbalance (QCM) is essentially a gravimetric device based on the piezoelectric effect that is able to transfer mechanical properties into electrical signals that can be detected and analyzed.

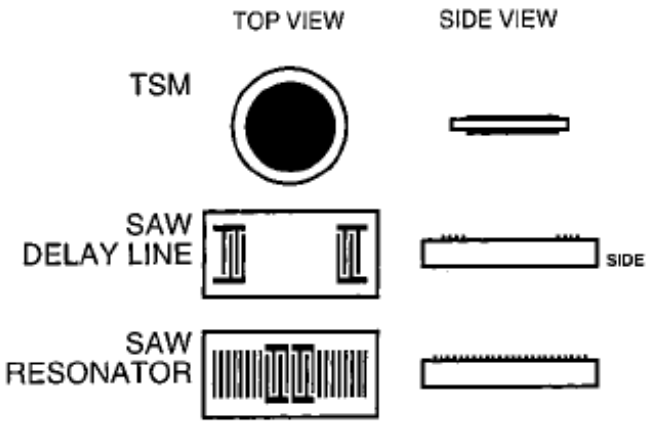

Figure 1-3. Figures of TSM and SAW sensors.

1.3.1 Brief History of QCM

In 1880, the QCM technique was first discovered by the Curie brothers, announcing that the signal transduction mechanism of QCM is based on the piezoelectric effect. After that, Lord Rayleigh showed that change of inertia of vibrating crystal results in the change of frequency. In 1959, Sauerbrey proposed an equation demonstrating a linear relationship of the resonant frequency and the mass deposited on the crystal, and QCM was first used in a sensing application involving moisture and volatile organic components, environmental pollutants, and gas-phase chromatography detectors. In the 1980s, the QCM was developed for other applications which operate in solution mode and a measure of the frequency changes were based on the changes in viscosity and density in liquid [9].

1.3.2 Characteristics of QCM

The main characteristic of QCM in the gas-phase application is to provide a transduction that is to transfer physical properties into measurable electronic signals that are able to be acquired by

electronic instruments. Theoretically, quartz crystal is used to manufacture different types of resonators, for example, thickness shear mode resonant, plate resonant, and flexural resonant, based on different angles of cutting on crystal, and their eigenfrequencies range from $5\times10^{2} \sim 3\times10^{8}$ Hz [8]. In the manufacturing of QCM, a raw quartz crystal is processed with AT-cut which is a cut with an angle of 35°10' with respect to the Z-axis or optical-axis. The advantage of the AT-cut quartz crystals is to make them fit for electronic devices because they possess a very high frequency stability, which minimizes a frequency fluctuation to $\Delta f / f \approx 10^{-8}$. Moreover, the temperature coefficient of AT-cut is almost zero which displays a best property for frequency resonant devices [8]. After the piece of AT-cut crystal is formed, the QCM is completed by depositing two gold electrodes on two sides of the crystal. Figure 1-4 [9, 8] illustrates the schematic outline of AT-cut and the manufacture of QCM with the two electrodes on both sides.

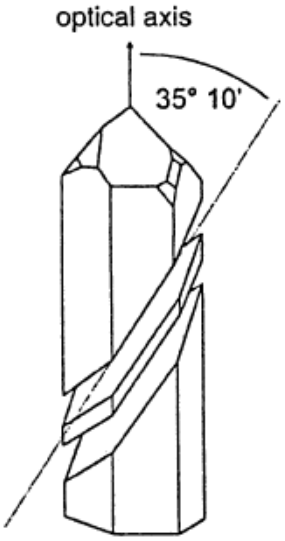

Figure 1-4 a. The schematic graph of the AT-cut crystal.

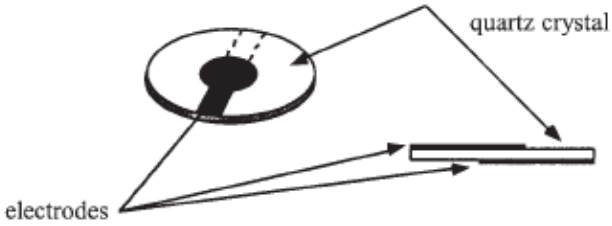

Figure 1-4 b. The schematic outline of QCM.

1.3.3 Oscillation/Resonant Frequency of QCM

The resonant oscillation of the QCM occurs when an ac voltage is simultaneously applied to the two electrodes on both upper and lower lattice surfaces. Figure 1-5 illustrates the mechanism of the electrical fields applied to the QCM and how the QCM oscillates [10]. Theoretically, there are different modes of oscillation in the quartz crystal and figure 1-6 [11] clearly shows a fundamental mode ($n=1$) and a third overtone mode ($n=3$) vibration for QCM devices. However, the QCMs in this discussion are based on the fundamental mode. The commercially available ranges of QCM resonant frequency are 5-20 MHz. Basically, the frequency range of QCM varies with the thickness of cutting, or the thickness of the QCM lattice. In other words, the resonant frequency of QCM will be increased when the cutting thickness is decreased; on the contrary, frequency will be decreased when the thickness is increased [8]. In application, the resonant frequency alters due not only to the cutting thickness of QCM but also to the mass that is deposited on the surface of QCM. The added mass that changes the resonant frequency are selective thin films coated on QCM or the gas molecules that are absorbed into the film or adsorbed onto the film. The reason why the additional mass alters the frequency is because of the increase in the thickness. A mathematical relationship between the added mass on the QCM and the change of resonant frequency is derived by Sauerbrey based on the condition of thin, rigid,

and uniform films, and published in 1959 [12] . The equation was then modified in the following [6]

$$\Delta f = -2 f_0^2 \frac{\Delta m}{A\sqrt{\rho\mu}} \qquad \text{Equation 1-1}$$

Where Δf (Hz) is the change in resonant frequency, f_0 (MHz) is the fundamental resonant frequency of the crystal, Δm (g) is the mass of the coating or material that attach on the surface of QCM and $A(cm^2)$ is the piezoelectric active area defined by the two gold electrodes, ρ is the density of quartz ($2.648\ g\ cm^{-3}$), μ is the shear modulus ($2.967\times10^{11}\ dyn\ cm^{-2}$).

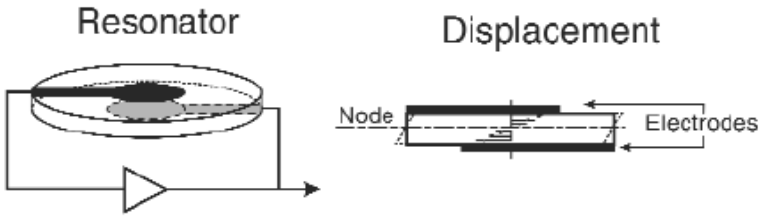

Figure 1-5. Oscillating mechanism of QCM sensor.

Since the value of ρ and μ are already known, equation 1-1 is simplified in the following equation

$$\Delta f = -2.26\times10^{-6} \times f_0^2 \frac{\Delta m}{A} \qquad \text{Equation 1-2}$$

Moreover, in order to discuss the mode of oscillation, Equation 1-2 can be expressed as

$$\Delta f_n = -2.26 \times 10^{-6} \times \frac{f_n^{\,2}}{n} \times \frac{\Delta m}{A} \qquad \text{Equation 1-3}$$

Where n represents the mode of oscillation. As depicted in the above cases, $n = 1$ represent the fundamental mode and the fundamental resonant frequency can be represented as f_0; $n = 3$ represent the third overtone mode and the resonant frequency can be written as f_3.

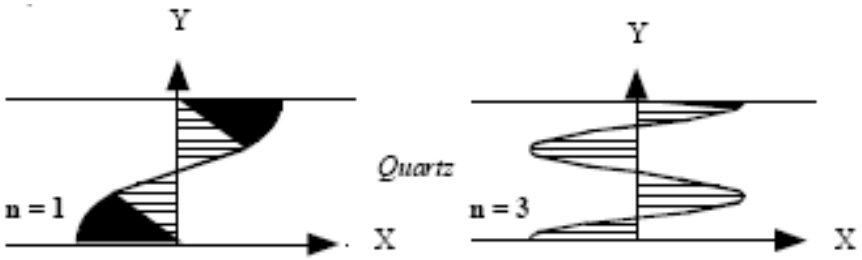

Figure 1-6. Fundamental mode and third mode of oscillation.

1.4 Piezoelectric Effect

Since the QCM is made from the quartz crystal, a piezoelectric material, QCM is considered as a kind of piezoelectric devices. Hence, the piezoelectric effect undoubtedly plays an important role in the application of QCM. The piezoelectric effect is a phenomenon that occurs when forces add on the crystal lattice and deform it. This effect can be observed from the current inside a circuit that is connected to the piezoelectric devices while a pressure makes the crystal to change its shape. The converse phenomenon called converse piezoelectric effect happens when an electronic field applied to the crystal induces a change of physical shape. For example, QCM

produces a resonant frequency response by repeatedly changing its relative position of upper and lower surfaces when an ac voltage is applied to the electrodes on the QCM [10].

CHAPTER 2

BACKGROUND RESEARCH

2.1 Coating Selection

Selective coatings or surface films are very thin material layers that are deposited on the one side or both sides of the crystal to accomplish the selectivity of adsorption or absorption of interested analytes [13]. Because the range of various coating materials extends as widely as analytes, the general concept has been to select a material for a particular analyte. However, since a full selectivity of a particular analyte is a very impossible goal, which means, it is impossible for a specific material to response to just one analyte, an alternative way to overcome the drawback of full selectivity involves the use of an array of sensors with partial selective coating [14]. Furthermore, in order to measure a maximum diversity of analytes, the concept of sensor array is also a significant design rather than just a single sensor in that the sensor array is designed to produce a signal array which is unique to a specific analyte. This way, analytes can be distinguished by different patterns of signal array. There are currently two most popular approaches to choosing proper coating materials from a wide variety of materials, one is Principal Component Analysis (PCA) and the other one is Linear Solvation Energy Relationship (LSER). The following sections will depict more detail about these two methods and relevant issues.

2.1.1 Sensor Selectivity

The meaning of selectivity of a sensor refers to that the degree of a sensor response to an interested analyte is free from the interference of another analyte contained in the sample. Accordingly, both selective films and the chemical properties of analytes are significant

components to selectivity. Generally speaking, selectivity is a measure of the relative contribution of a measurand to the changes of measured variables compared to the contributions of other substances [10].

2.1.2 Sensor Sensitivity

The sensitivity of a sensor is basically defined by the change of measured variables caused by a unit of analyte. In the case of TSM sensor, a calibration plot shown in figure 2-1 is introduced to explicitly describe the sensor sensitivity.

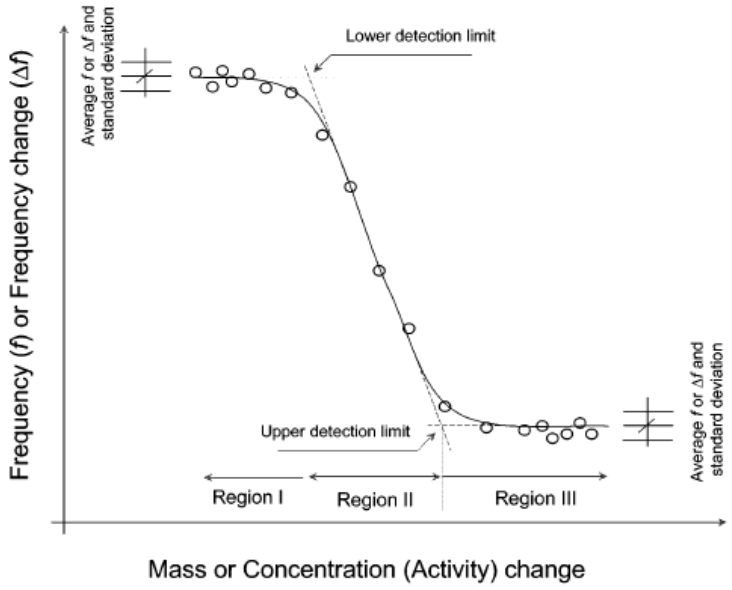

Figure 2-1. Calibration plot of QCM sensor.

Obviously, there are three theoretical regions that can depict the response of a TSM sensor under varying conditions. The lower detection limit between Region I and Region II is considered as a concentration point of the measured analyte for which the measured signal, or

measured frequency deviates from the range of standard deviation of the average signal value of low concentration in Region I. Like the lower detection limit, the upper detection limit between Region II and Region III is considered as another concentration point of the measured analyte for which the measured signal starts deviating from the limited range of standard deviation of the average signal value of high concentration in Region III. Hence, the linear concentration region locates between the lower detection and upper detection limits [10].

In the discussion of the sensitivity, the calibration plot is considered in the linear part and can be described by the following equation.

$$\Delta f = -C_f(\Delta M / A) \qquad \text{Equetion 2-1}$$

Where C_f represents the integral mass sensitivity and A represents the active area of the sensor.

Depending on the shape of the sensor, the integral mass sensitivity is derived differently from the differential mass sensitivity, $c_f = df/dm$. For a round shape TSM, the integral mass sensitivity is expressed as follows [10]

$$C_f = 2\pi \int_0^{r_c} c_f(r) r dr \qquad \text{Equation 2-2}$$

Where r_e is the electrode radius.

For a rectangular shape sensor, the integral mass sensitivity is expressed as follows [10]

$$C_f = \iint c_f(x, y)dxdy \qquad \text{Equation 2-3}$$

Where C_f is derived from a rectangular area with two dimensional axes x and y.

2.1.3 Principal Component Analysis (PCA) and Hierarchical Dendrogram

In sensor arrays, chemical diversity can be realized by selecting various materials having various chemical structures that provide a variety of properties and interactions, and now an approach to achieve such diversity is through the testing of great number of materials [7]. In the early gas research performed by Lawrence Livermore National Laboratory, techniques of pattern recognition were developed for the use of 27 quartz crystal sensors coated with different sensitive films which were chosen from a variety of materials based on stability, reversibility, selectivity and hydrophobic nature, and then exposed to 14 analytes. Moreover, the primary data used in their research were the shifts of frequency from the coated sensor responses. The data set of frequency shifts was used to form a matrix with variables of 27 coatings and samples of 14 analytes. Table 2-1 shows the data from measurements [14].

Table 2-1. The measured data of 14 analytes from 27 QCM sensors.

<ID no> Coating Materials	Benzene	Dodecane	DMMP	DM phosphate	1-butyl formate	Alpha-pinene oxide	Triphenyl phosphate	DIMP	Dichloro-pentane	Isopropyl acetate	Trimly phosphate	Octane	Triphenyl phosphate	Water
<1> Poly(butadieneacrylonitrile)	4	2	152	86	100	30	6	132	76	50	18	108	18	6
<2>Poly(p-vinylphenol)	22	9	74	155	83	22	8	34	40	14	14	30	20	19
<3>Poly(butadiene methacrylate)	51	12	60	68	97	30	23	46	48	41	31	134	42	55
<4>Polybutadiene hydroxy terminated	15	1	66	27	48	15	4	57	31	28	12	89	10	14
<5>Poly(vinyl stearate)	213	39	204	150	159	69	18	186	111	84	60	168	51	57
<6>Poly-1-butadiene	25	11	31	40	50	15	14	29	29	20	12	86	25	24
<7>Polybutadiene hydroxyl terminated liquid	14	3	90	52	56	25	4	88	49	36	17	97	10	10
<8>Methyl vinyl ether	11	8	12	36	30	7	9	10	13	5	0	26	17	29
<9>Octadecyl vinyl ether/maleic anhydride	16	46	108	63	38	33	5	134	23	25	21	119	16	27
<10>Polystyrene	1	1	11	25	27	6	9	8	2	21	4	4	0	13
<11>Poly vinyl isobutyl ether	7	10	21	16	34	47	8	27	7	31	16	4	8	22
<12>Poly(vinyl chloride)	0	3	50	17	41	0	28	32	47	9	12	0	0	58
<13>Poly-1-butene	0	10	4	10	17	15	18	8	5	21	3	17	0	10
<14>Poly(vinylcarbazole)	0	4	14	79	43	4	11	8	1	36	5	7	1	12
<15>Collodion	85	264	1589	1028	167	164	46	1956	121	171	114	370	66	72
<16>Poly(vinylbutyral)	9	13	34	45	54	7	19	22	5	37	10	14	3	23
<17>Poly(methyl methacrylate)	8	4	11	17	32	2	14	22	0	7	5	9	5	27
<18>Polyethylene	1	10	20	12	30	14	8	59	0	15	6	28	3	16
<19>Ethyl cellulose	10	20	19	26	42	28	9	59	60	7	16	5	2	23
<20>Poly(ethylene glycol methyl ether)	0	4	8	32	29	0	4	35	22	1	5	4	3	34
<21>Poly(caprolactone)	2	15	16	31	28	21	5	43	38	3	0	7	5	17
<22>Poly(caprolactone)triol	3	7	34	41	27	15	8	83	30	2	7	25	2	23
<23>Poly(caprolactone)triol 2X	7	4	16	63	12	10	6	35	59	0	2	5	3	27
<24>Carnuba wax	0	21	78	59	18	21	9	144	21	14	16	11	2	22
<25>Abietic acid	2	3	9	26	19	0	1	234	6	1	2	3	3	22
<26>DC 11	2	21	11	16	25	28	7	38	22	3	8	4	1	17
<27>Phenoxy resin	0	7	10	28	28	0	3	27	10	4	4	2	1	31

Principal Component Analysis (PCA) was first introduced by Carey, Kowalski and Beebe in 1986 to discriminate a wider range of gases using fewer sensors coated with sensitive materials. The original data derived from the Lawrence Livermore National Laboratory was utilized in PCA realization. The purpose of the PCA was to determine the possibility of reducing 27 original coated sensors without getting a significant loss of analytes identification information. The outcome of the PCA showed that seven principal components described at least 95% of the data information. The seven coatings recommended by [14] are listed in Table 2-2.

Table 2-2. Possible coating selection using PCA method.

ID No.	Component	% contribution
22	Poly(caprolactone)	7.1
3	Poly(butadiene methacrylate)	9.7
4	Polybutadiene hydroxyl terminated	11.0
11	Poly(vinyl isobutyl ether)	20.6
2	Poly(p-vinylphenol)	13.6
17	Poly(methyl chloride)	16.3
12	Poly(vinyl chloride)	47.4

Based on the interactions between analytes and coating materials, a variety of data are generated. The similarity of coating material can be analyzed using hierarchical cluster analysis that can be realized by grouping the data according to how similar their responses are across the data set, and then the result is plotted in a hierarchical dendrogram, as show in Figure 2-2 [7]. The hierarchical dendrogram illustrates hierarchical clusters for 27 sorbent coatings tested on thickness shear mode (TSM) films. In other words, 6 dissimilar coating groups represented by the letters “A” to “F” are results from 27 coatings and those coatings within the same group are similar. The hierarchical dendrogram is able to verify the results obtained from the PCA method

by showing that the coating selections of PCA are widely spread on different groups of the dendrogram, which indicates that both of the methods possess very similar criterion.

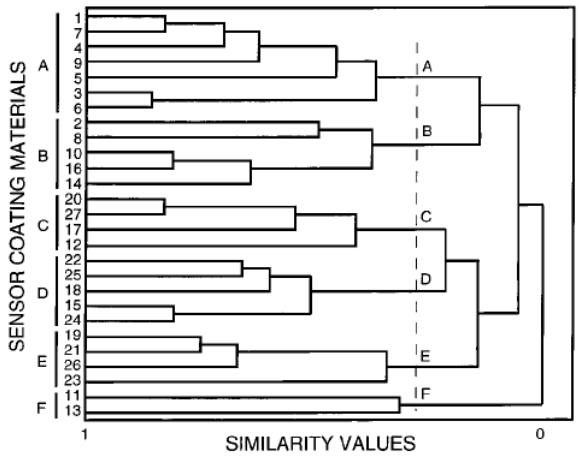

Figure 2-2. Hierarchical dendrogram showing 6 similar groups for 27 materials.

2.1.4 Linear Solvation Energy Relationship (LSER)

As mentioned in the above section, although PCA approach may provide sufficient diversity for successful chemical analysis, it does not guarantee that it is able to select a maximum diversity of coating space, for instance, the PCA does not include hydrogen bond acidic polymer [7]. Another approach to selecting a set of polymers that span all the coating space is suggested by the Linear Solvation Energy Relationship (LSER) approach which systematically considers the vapor sorption. The LSER that models interactions contributing to sorption and the value of the partition coefficient was first proposed by Jay W. Grate *et al* in 1988 and the coating selection based on LSER was described explicitly in 1991. The LSER equation was then induced as the following equation [7]

$$\log K = c + rR_2 + s\pi_2^H + a\Sigma\alpha_2^H + b\Sigma\beta_2^H + l\log L^{16} \qquad \text{Equation 2-2}$$

Where the coefficients (c, r, s, a, b, l) are related to sorbent polymers; a represents the sorbent phase hydrogen bond basicity; b represents the sorbent phase hydrogen bond acidity; s is related to the sorbent phase dipolarity/polarizablity; l is related to dispersion interactions; r is related to the ability of the phase to interact with solute n and π electron pairs and provides an indication of polarizability; c is from multiple linear regression used to obtain the LSER equation. The parameters ($R_2, \pi_2^H, \Sigma\alpha_2^H, \Sigma\beta_2^H, \log L^{16}$) characterize the solubility properties of vapors; R_2 provides a quantitative indication of polarizable n and p electrons; π_2^H measures the ability of a molecule to stabilize a neighboring charge or dipole; $\Sigma\alpha_2^H$ measures the hydrogen bond acidity; $\Sigma\beta_2^H$ measures the hydrogen bond basicity; $\log L^{16}$ is a combined measure of exoergic dispersion interactions [7].

According to the LSER equation, the first priority of the polymer selection includes the following functionalities [15]:

(a) Maximize dispersion interactions

(b) Maximize polarizability

(c) Maximize dipolarity (minimize basicity)

(d) Maximize basicity (minimize dipolarity)

(e) Maximize both basicity and dipolarity

(f) Maximize acidity (minimize basicity)

Based on the criterion of LSER form [7], the recommended polymer selection provided by Jay W. Grate is determined and listed in the following table 2-3 [7] which is considered a guideline for selecting a set of polymers spanning a wider range of gas chromatography.

Table 2-3. Polymer selection according to LSER method [7].

Interactions and properties	**Chemical structures, examples and comments**
Dispersion interactions	Alipoatic hydrocarbon polymers or substituents. Fluorination will decrease dispersion interactions. Poly(isobutylene) (PIB) and ploy(dimethylsiloxane) (PDMS) are useful examples. These are characterized by large l coefficients and are useful for sorbing aliphatic hydrocarbons or for distinguishing between members of a homologous series
Polarizability	Aromatic group increase polarizability relative to aliphatic groups. Phenyl-containing materials are useful, such as phenyl-substituted poly(siloxanes). Phenyl-substituted materials such as OV-25 (75% phenyl-25% methylpolysiloxane) are very good for sensitivity to chlorinated hydrocarbons and, in combination with aliphatic materials, help to distinguish between various low polarity vapors such as aliphatic hydrocarbons, aromatic hydrocarbons, and chlorinated hydrocarbons.
Dipolarity (minimize basicity)	Fluoroalkyl-substituted materials provide modest dipolarity without basicity. Fluoropropyl-substituted poly(siloxanes) such as OV-202 and OV-215 are candidate materials. However, the overall value of these weaky sorbent materials in arrays may not be great and will be application dependent.
Dipolarity allowing basicity	Nitrile groups are highly dipolar groups with only moderate basicity compared to many other high dipolar functional groups. Polysiloxanes with cyanopropyl (Silar 10C or SXCN) and cyanoalkyl (OV-275) groups are useful, and poly(ethylene maleate) (PEM) has also been found to have similar properties. These help to distinguish vapors with high dipolarity.
Basicity minimizing dipolarity	Aliphatic amines can provide basicity while minimizing dipolarity. In principle, poly(ethylenimine) (PEI) has secondary and tertiary amines, but typical commercial samples actually also have quaternary amines serving as ironic centers that interact with vapors with dipoles. This polymer has been poorly behaved in various sensor studies. Aminopropyl-substituted poly(siloxanes) are also candidates. Basicity favors interaction with hydroxyl-

	containing vapors such as organic acids and alcohols, and materials such as PEI are strong sorbents for water
Basicity and dipolarity	Many function groups are both very dipolar and very basic, including amades, urethanes, and sulfoxides. Like other basic materials, these sorb acids, alcohols and water. Poly(vinyl-pyrolidone) (PVP) for example, is a strong sorbent for water.
Hydrogen bond acidity	Fluorinated alcohols and phenols maximize hydrogen bond acidity and minimize basicity, while not having the basicity and self-association of carboxylic acids. Several materials have been synthesized to provide these properties including fluoropolyol (FPOL), a hexafluoro-2-propanol-substituted polysiloxane (SXFA), and fluorinated bisphenol materials (BSP3) and (BSP6). These materials are useful in detection of basic vapors including organophosphorus compounds.

The structure of the polymer is also a factor that is able to determine a diversity of properties including the solubility properties which can be provided by values of the LSER coefficients [7]. In their research, fourteen polymers selected to span coating space based on their structures were characterized at 298 K using LSER approach. Monomer structures of 12 polymers (Two of the 14 polymers were not considered due to poor physical properties) are shown in figure 2-3 [7].

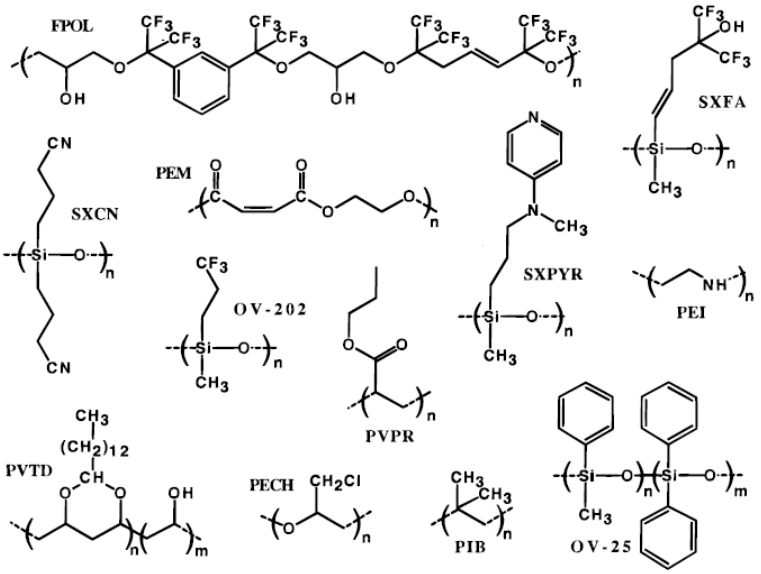

Figure 2-3. Monomer structures of 12 LSER polymers [7].

A potential array of six polymers according to LSER approach is suggested by Jay W. Grate and their values of LSER coefficients are listed in the Table 2-4.

Table 2-4. The values of LSER coefficients of suggested polymers [7].

Polymer	Polarizability(r)	Dipolarity/Polarizability(s)	Basicity(a)	Acidity(b)	Dispersion/Cacity(l)
PIB	-0.077	0.366	0.180	0.000	1.016
OV-25	0.177	1.287	0.556	0.440	0.885
OV-202	-0.480	1.298	0.441	0.705	0.807
PEM	-1.032	2.754	4.226	0.000	0.865
PEI	0.495	1.516	7.018	0.000	0.770
SXFA	-0.417	0.602	0.698	4.250	0.718

2.2 Sensor Coating

Generally, the noticeable ability that TSM sensor is able to perceive reactions while the measured substance is involving, contributes to the selected polymers deposited, or coated, on the surface of the TSM sensor. Because there is a wide variety of materials that can be used as selected polymers and the interaction of a specific polymer to different measured substances varies, the study of coating materials on the sensor surface has become an interesting research area on sensor development. According to recent research articles of coating process [16, 17], different topologies can cause different experimental measurements. For example, the different thicknesses of the coating material result in different responses of sensors under the same extrinsic condition (the same temperature, gas pressure and concentration). Currently, there are two popular coating approaches, spray coating and spin coating, used for the coating processes. These coating methods are introduced in the following sections.

2.2.1 Spray Coating

The spray coating is an easier and less expensive method to deposit the polymer onto the sensor substrate. In order to perform a proper coating, this method requires a steady supply of compressed air, a chamber for mixing the air and the polymer solution, and a good condition nozzle for the spray. The fabrication of a thin polymeric film begins with dissolving the selected polymer in a volatile solvent to become a polymer solution. The methodology of the coating is processed by brushing the sensor substrate with the mist of the polymer solution within a distance of approximately 10-15 centimeter between nozzle and substrate for 8-10 strokes [13]. The following diagram depicts the experimental setup for the spray coating.

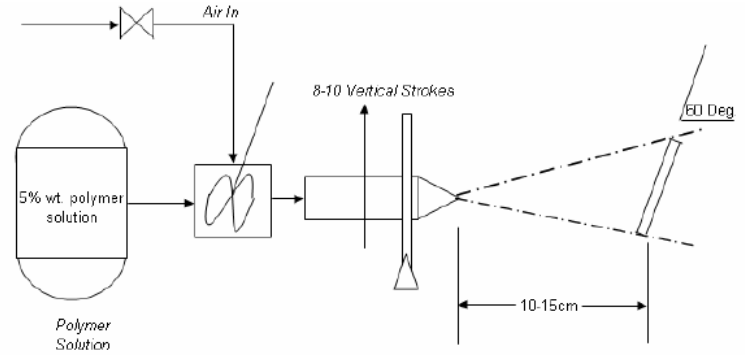

Figure 2-4. The experimental setup of spray coating [13].

A disadvantage of spray coating lies in its difficulty of controlling the thickness of the coated polymer on the sensor surface. Therefore, if the thickness of the polymer is an important factor of an experiment, this is not a proper method to coat the sensor. Contrary to this is that, should the thickness not be so important, spray coating would be a simple and time saving coating process [13].

2.2.2 Spin Coating

Spin coating is the other coating approach that is capable of reaching not only a uniform film but also a desired thin thickness. This process is realized by dropping a droplet of the polymer solution with a specific concentration onto the sensor substance and followed by spinning the sensor substance in a constant high speed for a given time. In this way, the droplet will spread out a uniform thickness while the solvent evaporates. Technically, the concentration of the polymer solution and the spinning speed are important factors in determining the thickness of the polymeric film deposited on the sensor. The lower concentration and the higher spinning speed result in a thicker film and the higher concentration and the lower spinning speed result in a thinner film.

2.3 TSM Sensor Limitation

2.3.1 Drift

During an experimental process, signal drift, a change of the measured signal of the TSM sensor without altering any experimental conditions, is inevitable. From the definition of [10], the drift is a slope of a linear function fitted in the data set which is located in the coordinate of the measured variable versus time. An example of signal drift is clearly displayed in the figure 2-4 [18].

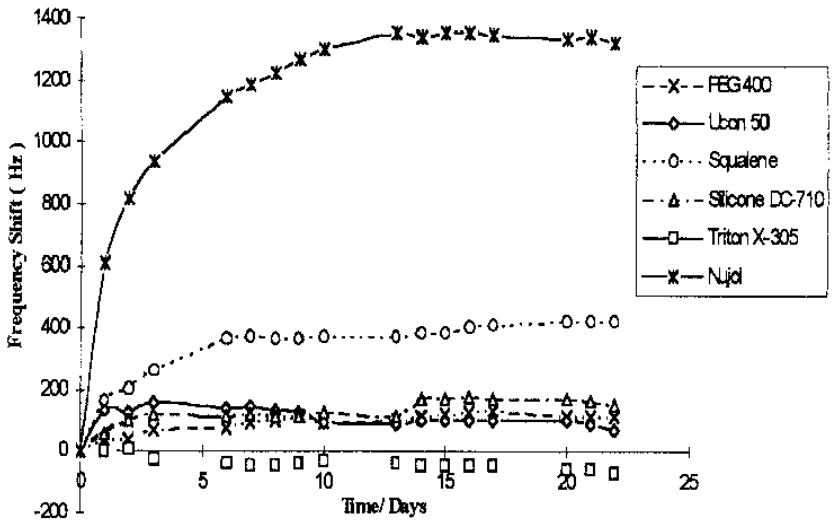

Figure 2-5. Signal drift in TSM sensors.

2.3.2 Hysteresis

Hysteresis is defined as the failure of the measured signal that has been altered through changes in ambient conditions to return to its original value when removing the alteration. Hence, hysteresis usually has kinetics origins. Nevertheless, reversible values of the measured signals are theoretically expected if the system has enough time to return to its initial condition [10].

2.3.3 Repeatability

Repeatability of the measured signal is determined in repeated experiments under the same conditions and the standard deviation of the measured signal is called repeatability [10]. According to International Organization for Standardization (ISO), the definition of repeatability is the precision under repeatability conditions where independent test results are obtained with the same method on identical items in the same laboratory by the same operators and equipments within short time intervals (ISO 3534-1). Moreover, repeatability of measurement results is

defined by International Union of Pure and Applied Chemistry (IUPAC) as the closeness of the agreement between the results of successive measurement of the same measured and carried out under the same conditions of measurement.

2.3.4 Reproducibility

According to International Organization for Standardization (ISO), the definition of reproducibility is the precision under reproducibility conditions where test results are obtained with the same method on identical items in different laboratories by different operators and different equipments (ISO 3534-1) [10].

CHAPTER 3

EXPERIMENTAL METHODS

3.1 QCM Sensor Design

The QCMs used in this research are 5MHz (part number 151223-5) as shown in the Figure 3-1, AT-cut with blank diameter of 0.538 inches and electrode diameter of 0.267 inches purchased from International Crystal Manufacturing (ICM). Although this type of QCM is mounted on a base with two small metal strips, the electrodes of the QCM are not bounded with strips for a convenience of separation for a process of spin coating.

Figure 3-1.Figure of 5MHz QCM sensor.

3.1.1 Selection of Experimental Polymers

According to the table 2-3 and availability, the polymers chosen for the sensor array are poly(isobutylene) (PIB) which maximizes the dispersion interactions, (75% phenyl-25% methylpolysioxane) (OV-25) which maximizes polarizability, Dicyanoalkylpolysiloxane (OV-275) which distinguishes high dipolarity, poly(ethylenimine) (PEI) which maximize basicity,

polyvinylpyrrolidone (PVP) which have both basicity and dipolarity, and BSP3 which maximizes the hydrogen bond acidity. Additionally, the reason for choosing the BSP3 polymer for maximizing the hydrogen bond acidity instead of other possible polymers (FPOL, SXFA and BSP6) is that BSP3 shows better sensitivity than other candidates [19].

3.1.2 Coating Process

As stating in chapter 2, there are two coating methods, spin coating and spray coating, for depositing interesting polymers on QCM sensors. For a condition of the same calibrated parameters, the thickness of every coated polymer in this research is design to be equal on QCM sensors. Hence, a coating method that is able to fabricate a desired thickness is a critical issue. Spin coating, therefore, becomes the only candidate of coating selection since spray is not able to control the coated thickness and also make the coated polymers uniform.

The thickness of coated polymer is a critical parameter that influences the response value of signals. Therefore, the desired thickness in this study is designed to be 400nm, which is reasonably and arbitrarily selected according to [16, 17]. The first step of coating polymers on QCMs is to dissolve polymers in proper solvents with a proper concentration. The concentration used between solute and solvent is volume-volume concentration (v/v) in this coating. According to different properties of the polymer, the concentration needed for each polymer solution is different in order to fabricate the same thickness. After a long testing process, the proper protocol is found. For PVP, 2% (v/v) concentration is made in chloroform. For OV-25, 9.9% (v/v) concentration is made in toluene. For PIB, 4% (v/v) concentration is made in hexane. For BSP3, 6.7% concentration is made in chloroform. For PEI, 8.8% (v/v) concentration is made in distilled

water. Unlike other polymer solutions, PVP and PIB solutions are additionally placed in a Sonicator and run through sonic pulses to break up the large particles of polymers to get a smoother coating. The coating process used a Photo-Resistant Spinner from Headway Research Inc. and spun QCMs at 2000 rpm for 60 seconds to produce polymeric films of 400nm. Those coated QCMs were then dried in a vacuum chamber except the OV-25 in that vacuum caused an inconsistent coating film. To measure the thickness of polymeric films, a Sloan Dektek IIA profilometer is used; a Gaertner L116S ellipsometer is also used for checking the measurement. All the coatings were done by Sandia National Lab except OV-275.

Table 3-1. Solvents and concentrations for making polymer solution for spin coating.

Polymer	Solvent	Concentration (v/v)
PVP	Chloroform	2.0% (v/v)
OV-275	Acetone	10.0% (v/v)
OV-25	Toluene	9.9% (v/v)
PIB	Hexane	4.0% (v/v)
BSP3	Chloroform	6.7% (v/v)
PEI	Distilled Water	8.8% (v/v)

The OV-275 coating was fabricated by the cooperation of the Laboratory for Industrial Metrology and Automation (LIMA), Nanomaterials Integration Laborotary and Chemistry department. To fabricate 400nm polymer, 10% (v/v) concentration is made in acetone and the QCM is also spun at 2000 rpm for 60 seconds. The thickness is measured using a profilometer. The summary of the protocol for 400nm thickness is showed in the table 3-1. When processing

the spin coating, the conduction between gold conductor on the crystal and the QCM holder cannot be block.

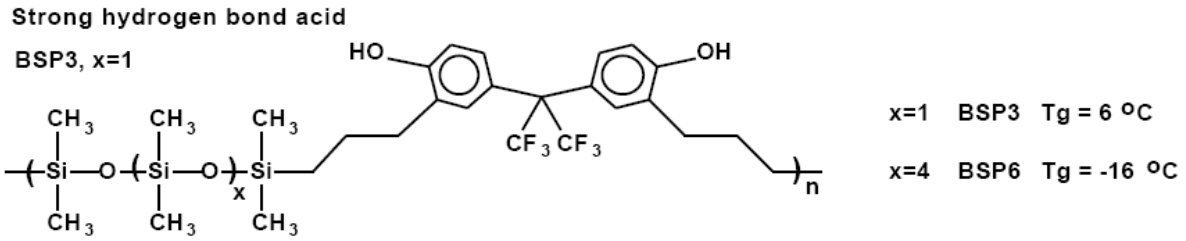

Figure 3-2 a. Monomer structure of both BSP3 and BSP6 [20].

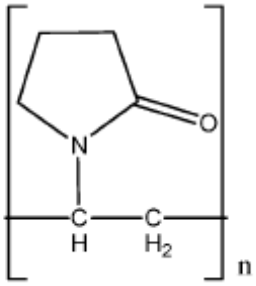

Figure 3-2 b. Monomer structure of PVP [21].

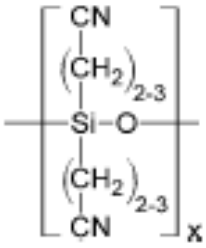

Figure 3-2 c. Monomer structure of OV-275 [21].

The used polymers were from different sources. The low molecular weight PIB and 50% solution of PEI in water came from Aldrich Chemical Company Inc., PVP came from Scientific

Polymer Inc., the OV-25 and OV-275 came from Ohio Valley Specialty, and the BSP3 came from Oxazogen. The monomer structures of PEI, PIB and OV-25 are shown in Figure 2-3; the Figure 3-2 shows the monomer structure of other polymers, BSP3, PVP, and OV-275.

3.2 Similarity Measure

In many applications, similarity measure algorithm has been considered as a useful tool to deal with the issue of pattern classification of unknown patterns. Based on fuzzy set theory, fuzzy similarity measure is one of the approaches to deal with the pattern classification.

3.2.1 Fuzzy Set Theory

Before going into the fuzzy set theory, classical set is worth to be discussed since fuzzy set is basically extended from classical set. In classical set theory, all elements in a set belong to only one classification, a membership or a non-membership, and the differentiation between the membership and the non-membership is very clear and unambiguous. For example, ages above 70 years old is considered as “old” and ages below 7 years old is considered as “not old” or “young”. Clearly, the linguistic term “age” is in just one classification, “old” membership or “young” membership. If a man with 70 years old is considered “old”, what should the man with 69 years old man be considered? According to the above statement, the 69 years old man is neither “old” nor “young” because the “old” membership exactly defines ages over 70 years old as “old” and below 7 years old as “not old”. This expression is correct in mathematic inference but obviously cannot be reasonably accepted by normal logic. Fuzzy set theory then is designed to deal with this logic conflict. More examples of classical set are: a lock is either “on” or “off”, a book is either “open” or “close”, the high of a man is either “tall” or “short”, the condition of a

product is either “good” or “bad” and so on. For any classical set C, the characteristic function is expressed as the following

$$\mu_C(x) = \begin{cases} 1 & iff\ x \in C \\ 0 & iff\ x \notin C \end{cases} \qquad \text{Equation 3-1}$$

where iff represents the abbreviation of *if and only if* [23, 24].

The concept of fuzzy set theory was first proposed by Zadeh in 1965 [25]. Fuzzy set is a set of vagueness as the name indicates. For example, let A be the universe set of human age, and Ao be the subset of A. Giving that $Ao = \{ a \in A \mid a \text{ is old} \}$, then Ao is a fuzzy set since it is vague in the mathematic measure and is not well defined. Different from classical set theory, fuzzy set theory introduces an idea of continuum amount elements within the set. All elements in the set are characterized by membership functions. The membership function of a fuzzy set S is usually represented as $\mu_S(x)$ which has the minimum value of 0 and maximum value of 1, and can also be values varying from 0 to 1. Figures 3-3 and 3-4 are membership functions for the example of “old” and “young” membership stated above. In the case of Figure 3-3, the age of 70 years old is said to be “old” with a grade of 0.78 and the age of 69 years old is said to be “old” with a grade of 0.77. Hence, the age of 69 years old is no more undefined. However, the fuzzy set can be characterized not only by a specific membership function but different membership functions. In the case of Figure 3-4, the age is characterized by “young” membership function and 70 years old has a grade of 0.33 and 69 years old has a grade of 0.34. Other than these two membership functions, more membership functions with different definitions and curve shapes can be added. For example, “middle young” and “middle old”.

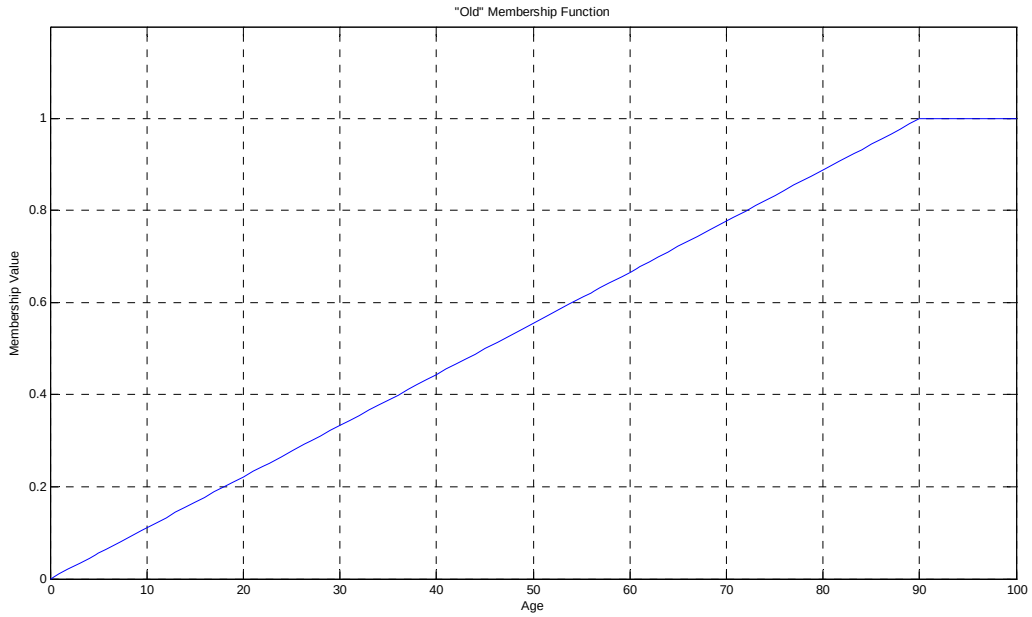

Figure 3-3. The membership function of fuzzy set “old”.

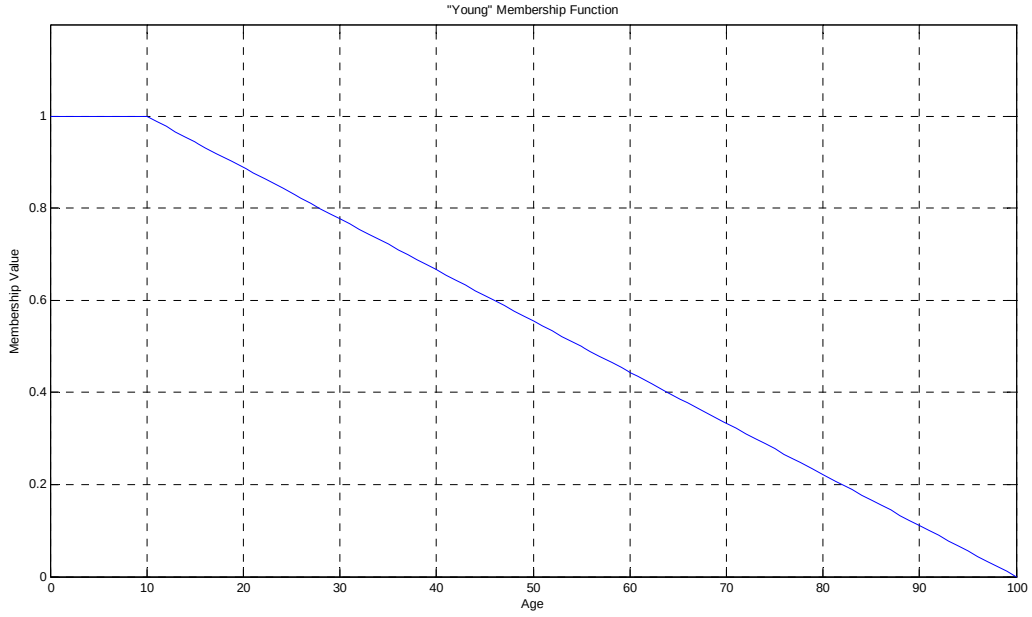

Figure 3-4. The membership function of fuzzy set “young”.

Usually, the shape of the membership function varies according to the user design. The frequently used curves are shown below [23].

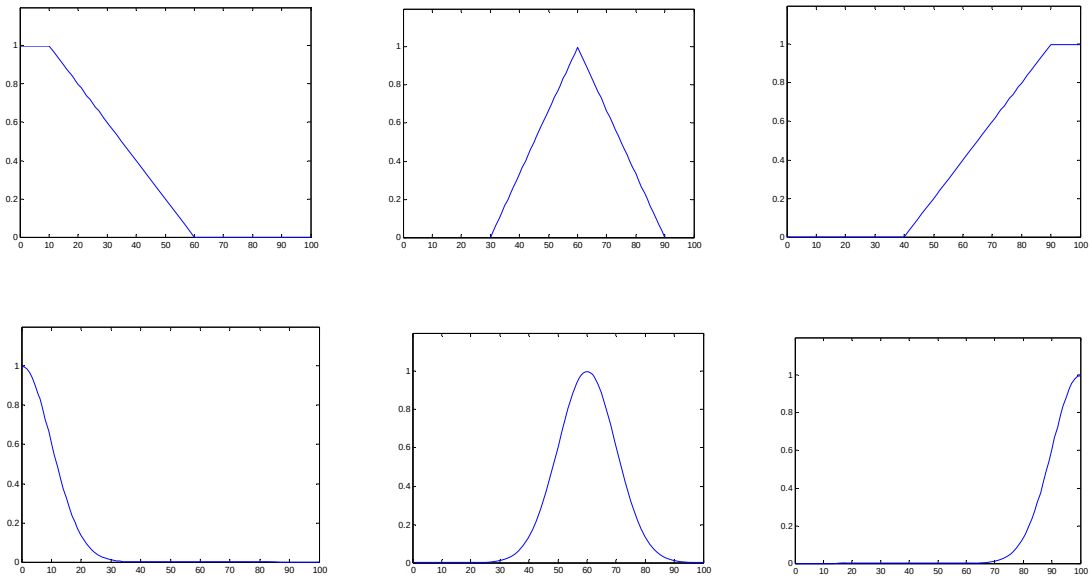

Figure 3-5. Various shape of membership function.

3.2.2 Fuzzy Sets Mathematic Operations

According to [23, 24, 25], the mathematical operation of fuzzy set is basically extended from the original set theory. The definition and detail operation is listed in the following.

Empty:

A fuzzy set is empty if and only if the grade of its membership function in the defined set S is zero. $\mu(x) = 0$, for all $x \in X$.

Equality:

Let A and B be two fuzzy sets and $x \in X$, then $A = B$ if and only if $\mu_A(x) = \mu_B(x)$ for all $x \in X$.

Containment:

Let A and B be two fuzzy sets, then A is contained in B ($A \subset B$) if and only if $\mu_A(x) \leq \mu_B(x)$ for all $x \in X$.

Intersection (and):

$\mu_{A \wedge B}(x) = \mu_A(x) \wedge \mu_B(x) = \min(\mu_A(x), \mu_B(x))$, for all $x \in X$. The notation $\wedge$ based on two valued logic is also called "*and*" operator.

Union (or):

$\mu_{A \vee B}(x) = \mu_A(x) \vee \mu_B(x) = \max(\mu_A(x), \mu_B(x))$, for all $x \in X$. The notation $\vee$ based on two valued logic is also called "*or*" operator.

Complement (not):

$\mu_{\bar{A}}(x) = 1 - \mu_A(x)$

3.2.3 Fuzzy Similarity Measure

Fuzzy similarity measurement designed to distinct analytes associated with their own signal patterns is an algorithm based on the fuzzy membership function. Let A and B be two fuzzy sets and the similarity of them is denoted by $S(A,B)$. The value of $S(A,B)$ is between 0 and 1 according to how similar the two sets are. If $S(A,B) = 0$, A and B are totally dissimilar. If $S(A,B) = 1$, A and B are identical. The algorithm is originally derived from the basic operation of fuzzy set [26],

$$S(A,B) = \frac{|A \cap B|}{|A \cup B|} \qquad \text{Equation 3-2}$$

where $|\bullet|$, $\cap$ and $\cup$ represent the cardinality, intersection and union in the regular set.

Equation 3-2 can be converted into the expression of membership function. Let $X = \{ x_i \mid i = 1, 2, 3, \ldots, k \}$, then $S(A,B)$ is expressed as equation 3-3 and equation 3-4

$$S(A,B) = \frac{\sum_{i=1}^{k} [\mu_A(x_i) \wedge \mu_B(x_i)]}{\sum_{i=1}^{k} [\mu_A(x_i) \vee \mu_B(x_i)]} \qquad \text{Equation 3-3}$$

$$S(A,B) = \frac{\sum \min[\mu_A(x_i), \mu_B(x_i)]}{\sum \max[\mu_A(x_i), \mu_B(x_i)]} \qquad \text{Equation 3-4}$$

where $\wedge$ and $\vee$ represent operators of “and” and “or” in the fuzzy membership.

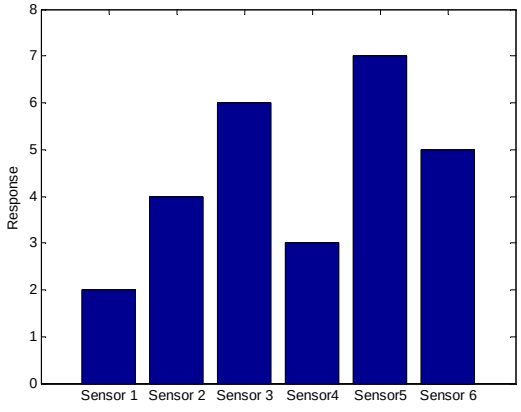

Figure 3-6. Example of signal bar chart.

Fuzzy similarity measurement expressed in equations 3-2, 3-3 and 3-4 can further be modified for the application of signal pattern recognition. Usually, the signal responses of QCM sensors are displayed with the bar chart as shown in Figure 3-6. Each response from a single sensor is called the "feature" of the sensor to a measured analyte and the combination of those "feature" is called the signal pattern of the measured analyte. Therefore, different analytes result in different signal patterns [20].

The modified fuzzy similarity is based on operating the values of the "feature" instead of the value of membership function. Let A and B be two signal patterns, $A = \{ a_i \mid i = 1, 2, 3, \ldots, k \}$ and $B = \{ b_i \mid i = 1, 2, 3, \ldots, k \}$. The fuzzy similarity of these two patterns is expressed as [18, 27]

$$SF(A,B) = \frac{\sum \min(a_i, b_i)}{\sum \max(a_i, b_i)} \qquad \text{Equation 3-5}$$

3.3 Concentration Effect

The magnitude of a TSM sensor response depends not only on the thickness of the polymer coated on the surface of the sensor but also on the concentration of the gas present in the environment. Therefore, apart from the polymer thickness that has been considered as a design factor, gas concentration is also a crucial issue worthy to be discussed. Theoretically, an increase of gas concentration causes more molecules to attach onto the sensor surface; thus resulting in a heavier load of weight on sensors and also amplifies the sensor response. Figure 3-7 illustrates the calibration graphs of TSM sensors coated with PDMS and also displays the influence of the concentration effect [17]. Even though Figure 3-7 shows a perfect linear response with respect to

the concentration, most calibration graphs, however, show non-linear sensor responses [17, 28, 29].

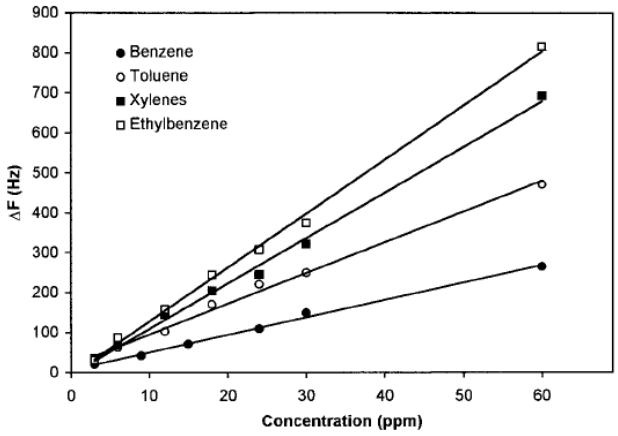

Figure 3-7. TSM sensor responds to different analytes with different concentrations.

3.4 Problem State

As stated in chapter 1, the response of a sensor is theoretically caused by the mass of the interested gas attached onto the coated sensor. The beauty of similarity measurement is to enable the sensor array to distinguish or "smell" the measured analyte. However, according to section 3.3, the response of a sensor to a specific gas can vary due to the changes of the gas concentration; this situation can occur in all chemical components. In other words, the similarity method based on the pure gas or 100% interested gas will be invalid when the measured gas is mixed with other unknown chemical components. To overcome this problem, this research suggests that more database of mixed gases are needed to be established other than just pure gas database.

CHAPTER 4

EXPERIMENTAL PROCESSES

4.1 Experimental Setup

This research is designed to use the nitrogen (N_2) as a reference gas since it occupies approximately 78% of the total gases in the surrounding atmosphere. Three interested gases, oxygen (O_2), helium (He) and argon (Ar), according to availability are mixed into the reference gas (N_2) respectively for the purpose of establishing a database of various concentrations. Once the database is built, testing gases with different concentrations will be examined.

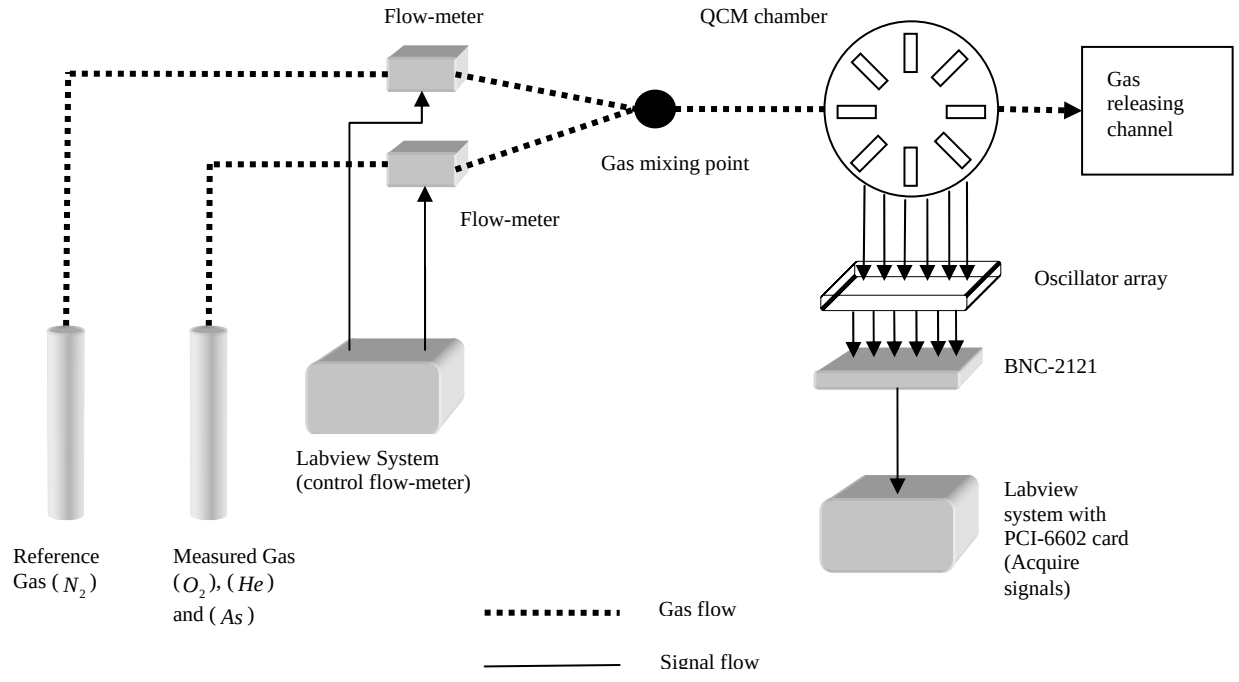

Figure 4-1. Experimental setup for electronic nose.

Figure 4-1 illustrates the significant outline of the experimental setup. To precisely produce a needed gas, two flow-meters are controlled by Labview program for the purposes of properly mixing gases in a correct percentage. The mixed gas is introduced into a chamber where six QCMs are installed, as shown in figure 4-2, and then released from an outlet channel. However there is a limitation existing in the two flow-meters. The limitation restricts the range of the mixing ratio which is not able to produce a percentage of above 55% and below 100% due to the existing condition of the Labview system. In other words, the mixing ratios that can be produced are from 0% (pure reference gas) to 55% and just 100% (pure measured gas).

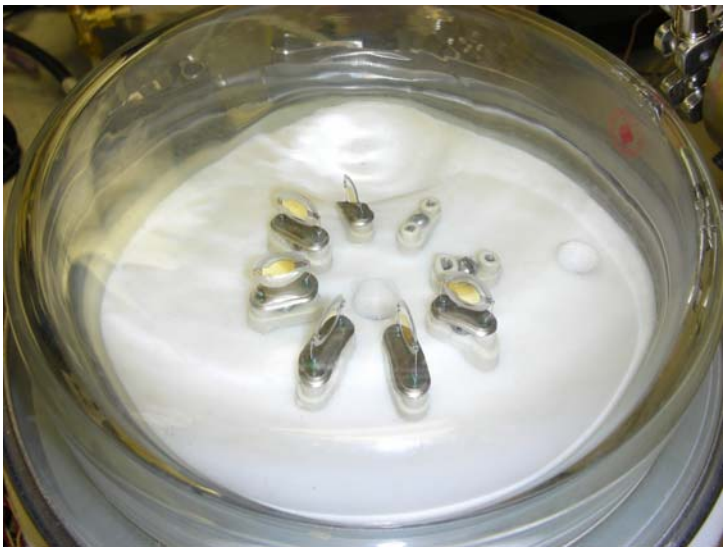

Figure 4-2. The gas chamber with six 5MHz QCMs installed inside.

The main body of QCM chamber is made from Teflon since Teflon material has an inert property to chemicals, and the top of the chamber is made from glass that is able to be clamped to the main body of the chamber. A V-Band clamp is used to tightly seal the chamber. The main body of the chamber has eight QCM holders which are connected with conductive wires

extending to outside of the chamber. Figure 4-3 shows the exact components of the chamber: the main body, glassy top, V-Band clamp, QCM holders, and conductive wires. Nevertheless, a limitation appears on the chamber. Because the age of the chamber, it is not able to be perfectly sealed if a vacuum is applied and damage on the chamber could happen. Therefore, this experiment is designed not to use a vacuum pump to flush gases.

Figure 4-3. The designed QCM chamber used for filling with gases.

The task of acquiring responding signal from the oscillator is accomplished by the cooperation of NI PCI-6602 card, BNC-2121 and Labview, which are purchased from National Instruments Corporation. The NI PCI-6602 is installed on the PCI slot in a computer which has a Labview program installed. The BNC-2121 connected to PCI-6602 card provides BNC and conductive wire connections that are capable to other instruments. Six QCMs coated with different polymers are installed in the chamber and are connected to an oscillator array which is supported by 5V DC power. The BNC-2121 is connected with oscillator array to acquire signals

generated by oscillator array. Figure 4-4 displays the detail connection of QCM the chamber on the top left, oscillator array under the QCM chamber, and BNC-2121 on the bottom right.

In order to measure signals from the above setup and control NI equipments, Labview is used as a software program and the designed interface is shown in Figure 4-5. Due to the limitation of the PCI-6602 card, only three channels can simultaneously be measured instead of six channels for all the sensors. Hence, the measurement for six sensors is separated into two groups; the first group is designed to measure sensors coated with BSP3, PIB, and OV-25; the second group is designed to measure sensors coated with PEI, PVP, and OV-275. From Figure 4-5, it is clear that the first group is located on the left column and second group is on the right. Therefore, when measuring one group, the other group will not have responses.

Figure 4-4. The connection of QCM chamber, oscillator array and BNC-2121.

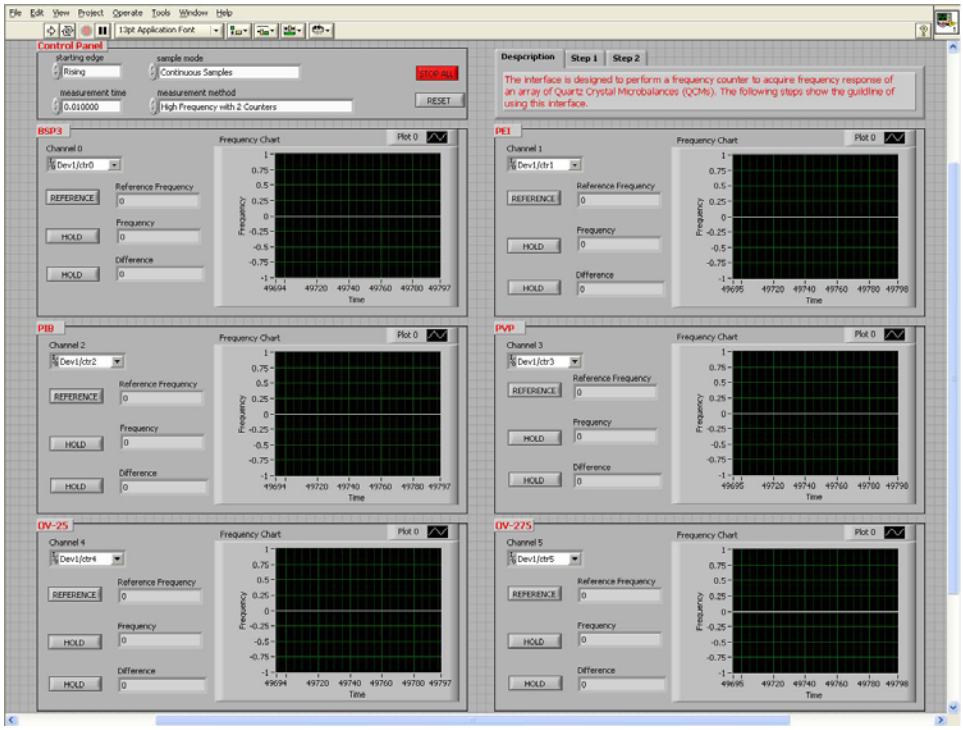

4-5. Designed Labview interface for data acquisition.

Three limitations mentioned above are concluded here. First, the flow-meters used produce the range of gas concentrations from 0% (pure reference gas) to 55% and just 100% (pure measured gas). Second, vacuum chamber can not be used due to the age of the chamber. Third, NI PCI-6602 card measures only three sensors simultaneously instead of six sensors.

4.2 Data Acquisition

According to the operational property of the QCM sensor, the data to be acquired is the change of the frequency with respect to the frequency of the reference gas. The experiment starts with collecting the actually frequency of the three interested gases (Oxygen, Helium, and Argon) with percentages of 100% (pure interested gas), 55 %, 50 %, 45%, 40%, 35%, 30%, 25%, 20%, 15%, 10%, and 0% (pure reference gas). Each percentage is measured three times and an average

is completed to obtain average frequencies. Due to the limited amount of gases, this experiment measures only three times of each gas percentage. Figures 4-6 and 4-7 show responses of groups I and II. From these two group responses, the signal form the QCMs coated with BSP3, PIB, PEI and PVP are very stable and the fluctuation of the signals is about 1 or 2 Hz, which is far smaller than the signals. However, the signals from the QCMs coated with polymer OV-25 and OV-275 are unstable and fluctuate greatly. The cause of these unstable signals comes from the physical property of both polymers. These two polymers coated on the surface of QCM exhibit viscous fluid phase instead of rigid phase as other polymers (BSP3, PIB, PEI and PVP). This phenomenon explains that the force of the chemical bonding between the polymer molecules is not strong enough to allow both polymers stay in the rigid phase.

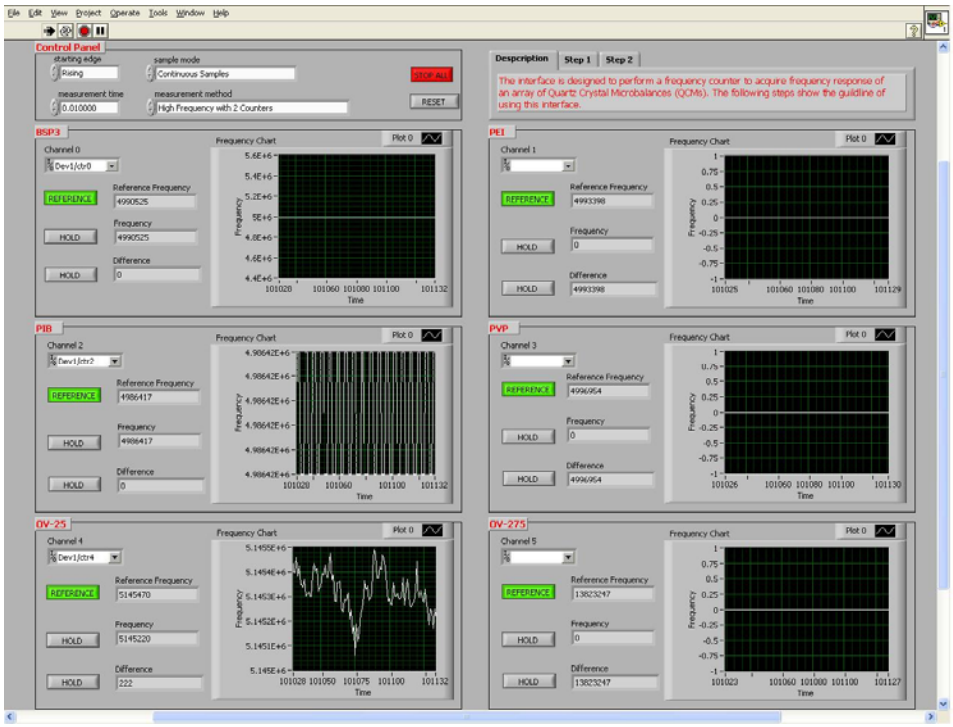

Figure 4-6. Responses of group I (include BSP3, PIB and OV-25).

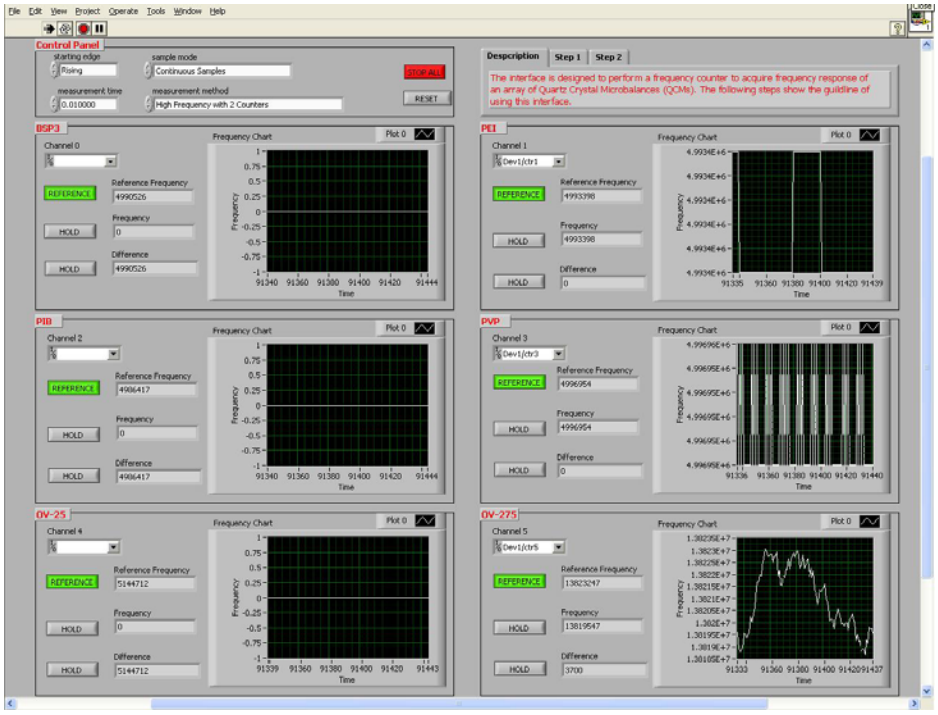

Figure 4-7. Responses of group II (include PEI, PVP and OV-275).

4.3 Database Design

Once the data of every concentration are recorded, a database can be established by calculating the difference of the frequencies of each concentration with respect to the frequency of the reference gas. Since sensors with polymer OV-25 and OV-275 do not respond well, the database is built based on only the sensors with BSP3, PIB, PEI and PVP.

Testing data is acquired in the same way as stated in section 4.2 and frequency differences are then calculated in order to compare their similarity.

CHAPTER 5

EXPERIMENTAL RESULT AND CONCLUSION

5.1 Result of Fuzzy Similarity Calculation

As stated in section 3.2.3, the fuzzy similarity measure for signal patterns can be realized by utilizing equation 3.5 and the value of the measurement $SF(A,B)$ between two patterns A and B is in the range from 0 to 1. The feature of signal pattern is the difference of the frequency of each sensor. Tested gases are 10%, 20%, 30%, 40% and 50% of each gas and results are shown from table 5-1 to table 5-15.

Table 5-1. The result of testing 10% oxygen.

	10%	15%	20%	25%	30%	35%	40%	45%	50%	55%	100%
Oxygen	0.3551	0.4432	0.3012	0.2321	0.1866	0.1453	0.1122	0.0751	0.0553	0.0447	0.0276
Helium	0.7319	**0.7514**	0.5455	0.4083	0.335	0.2456	0.1835	0.1468	0.1216	0.106	0.0728
Argon	0.1616	0.249	0.3488	0.4094	0.4921	0.4278	0.3756	0.3216	0.2737	0.2216	0.15

Testing Gas: 10% oxygen Result: 15% helium

Table 5-2. The result of testing 20% oxygen.

	10%	15%	20%	25%	30%	35%	40%	45%	50%	55%	100%
Oxygen	0.3146	0.8093	**0.8224**	0.6339	0.5096	0.3966	0.3065	0.2052	0.1511	0.1221	0.0755
Helium	0.3609	0.5632	0.6215	0.5889	0.5543	0.4644	0.3471	0.2777	0.2318	0.202	0.1377
Argon	0.2387	0.4574	0.6797	0.6628	0.5402	0.4643	0.4	0.3571	0.3032	0.2453	0.1658

Testing Gas: 20% oxygen Result: 20% oxygen

Table 5-3. The result of testing 30% oxygen.

	10%	15%	20%	25%	30%	35%	40%	45%	50%	55%	100%
Oxygen	0.1731	0.4473	0.648	0.835	**0.8986**	0.7111	0.5568	0.3728	0.2745	0.2219	0.1355
Helium	0.2074	0.3371	0.476	0.6261	0.6245	0.5415	0.5625	0.45	0.3757	0.3274	0.2231
Argon	0.1144	0.2227	0.3147	0.3155	0.3229	0.3428	0.3495	0.3347	0.2842	0.2368	0.1597

Testing Gas: 30% oxygen Result: 30% oxygen

Table 5-4. The result of testing 40% oxygen.

	10%	15%	20%	25%	30%	35%	40%	45%	50%	55%	100%
Oxygen	0.1015	0.2667	0.3924	0.5068	0.6333	0.8109	**0.8715**	0.6358	0.4681	0.3777	0.2307
Helium	0.1321	0.214	0.3144	0.4126	0.4734	0.5286	0.6399	0.6918	0.6181	0.5387	0.3671
Argon	0.1029	0.2033	0.3245	0.411	0.4889	0.4925	0.4861	0.4748	0.4756	0.4704	0.4208

Testing Gas: 40% oxygen Result: 40% oxygen

Table 5-5. The result of testing 50% oxygen.

	10%	15%	20%	25%	30%	35%	40%	45%	50%	55%	100%
Oxygen	0.0711	0.1868	0.2749	0.3567	0.4437	0.5701	0.7378	**0.8893**	0.6669	0.534	0.329
Helium	0.0977	0.1569	0.2434	0.3213	0.3681	0.4167	0.5713	0.7079	0.736	0.7421	0.5158
Argon	0.0693	0.1332	0.2107	0.2656	0.3273	0.401	0.4779	0.5108	0.5089	0.4984	0.5595

Testing Gas: 50% oxygen Result: 45% oxygen

Table 5-6. The result of testing 10% helium.

	10%	15%	20%	25%	30%	35%	40%	45%	50%	55%	100%
Oxygen	0.2667	0.3842	0.3037	0.2473	0.1969	0.1661	0.1393	0.1005	0.0796	0.0626	0.041
Helium	**0.6545**	0.4709	0.3202	0.2396	0.1966	0.1441	0.1077	0.0862	0.0719	0.0627	0.0427
Argon	0.2753	0.3645	0.453	0.524	0.6022	0.5062	0.4282	0.3811	0.3186	0.2578	0.1705

Testing Gas: 10% helium Result: 10% helium

Table 5-7. The result of testing 20% helium.

	10%	15%	20%	25%	30%	35%	40%	45%	50%	55%	100%
Oxygen	0.3436	**0.6416**	0.5495	0.4429	0.3562	0.2933	0.2396	0.1687	0.1303	0.1036	0.0664
Helium	0.4301	0.5674	0.52	0.4882	0.4005	0.2936	0.2194	0.1755	0.1465	0.1277	0.087
Argon	0.3268	0.4624	0.549	0.6227	0.513	0.4317	0.3655	0.3256	0.2725	0.2205	0.1455

Testing Gas: 20% helium Result: 15% oxygen

Table 5-8. The result of testing 30% helium.

	10%	15%	20%	25%	30%	35%	40%	45%	50%	55%	100%
Oxygen	0.2628	0.556	0.6743	0.593	0.4791	0.3919	0.3176	0.2221	0.1701	0.1358	0.0876
Helium	0.3416	0.4596	0.6483	0.6366	0.5461	0.4004	0.2992	0.2394	0.1998	0.1741	0.1187
Argon	0.4505	**0.7295**	0.6506	0.4789	0.3722	0.3135	0.2658	0.2372	0.1988	0.1607	0.1053

Testing Gas: 30% helium Result: 15% argon

Table 5-9. The result of testing 40% helium.

	10%	15%	20%	25%	30%	35%	40%	45%	50%	55%	100%
Oxygen	0.1551	0.4074	0.5995	0.7778	**0.8559**	0.6941	0.5502	0.3777	0.2863	0.2308	0.1526
Helium	0.2206	0.3004	0.4246	0.5738	0.6599	0.5696	0.5426	0.434	0.3623	0.3158	0.2152
Argon	0.2976	0.4408	0.4977	0.5184	0.518	0.5159	0.4424	0.3891	0.3216	0.2555	0.1709

Testing Gas: 40% helium Result: 30% oxygen

Table 5-10. The result of testing 50% helium.

	10%	15%	20%	25%	30%	35%	40%	45%	50%	55%	100%
Oxygen	0.0893	0.2347	0.3453	0.448	0.5573	0.716	**0.8669**	0.6948	0.5211	0.4203	0.2639
Helium	0.1035	0.1539	0.2301	0.3208	0.3788	0.4372	0.607	0.66	0.6394	0.5573	0.3797
Argon	0.0927	0.189	0.3053	0.3882	0.4805	0.5706	0.5579	0.5417	0.5364	0.5282	0.5135

Testing Gas: 50% helium Result: 40% oxygen

Table 5-11. The result of testing 10% argon.

	10%	15%	20%	25%	30%	35%	40%	45%	50%	55%	100%
Oxygen	0.1976	0.3807	0.4839	0.5734	0.621	0.5077	0.4106	0.2881	0.2214	0.1755	0.115
Helium	0.3016	0.3983	0.5525	0.7116	0.7332	0.5498	0.4109	0.3287	0.2744	0.2392	0.163
Argon	**0.7361**	0.6667	0.4337	0.3478	0.2654	0.2236	0.1898	0.1589	0.1315	0.0994	0.0667

Testing Gas: 10% argon Result: 10% argon

Table 5-12. The result of testing 20% argon.

	10%	15%	20%	25%	30%	35%	40%	45%	50%	55%	100%
Oxygen	0.146	0.3834	0.5643	0.6667	0.7062	0.7143	0.5744	0.4004	0.3052	0.2432	0.156
Helium	0.2156	0.2953	0.4149	0.5589	0.6426	0.694	0.5705	0.4564	0.3798	0.331	0.2263
Argon	0.2677	0.5202	0.802	**0.8578**	0.7235	0.5956	0.5106	0.4332	0.3621	0.289	0.1917

Testing Gas: 20% argon Result: 25% argon

Table 5-13. The result of testing 30% argon.

	10%	15%	20%	25%	30%	35%	40%	45%	50%	55%	100%
Oxygen	0.1182	0.3104	0.4568	0.5926	0.6895	0.758	0.7077	0.493	0.3748	0.2998	0.1928
Helium	0.1793	0.2527	0.3527	0.4731	0.5456	0.602	0.7095	0.5696	0.4717	0.4113	0.2819
Argon	0.1767	0.3344	0.5179	0.69	0.8567	**0.8628**	0.7804	0.6682	0.5545	0.44	0.2961

Testing Gas: 30% argon Result: 35% argon

Table 5-14. The result of testing 40% argon.

	10%	15%	20%	25%	30%	35%	40%	45%	50%	55%	100%
Oxygen	0.1015	0.2667	0.3924	0.5091	0.6333	0.7248	0.7829	0.5795	0.4395	0.3521	0.2243
Helium	0.1476	0.217	0.3043	0.409	0.4738	0.5243	0.734	0.6631	0.5499	0.4796	0.3288
Argon	0.1328	0.2582	0.402	0.5188	0.6441	0.7795	**0.9156**	0.837	0.7273	0.585	0.3913

Testing Gas: 40% argon Result: 40% argon

Table 5-15. The result of testing 50% argon.

	10%	15%	20%	25%	30%	35%	40%	45%	50%	55%	100%
Oxygen	0.0856	0.2248	0.3308	0.4291	0.5338	0.6858	0.745	0.6892	0.5219	0.4189	0.2648
Helium	0.1193	0.1844	0.2528	0.3436	0.4002	0.4482	0.6306	0.7311	0.6497	0.567	0.3891
Argon	0.1004	0.1951	0.3119	0.392	0.4867	0.589	0.7064	0.803	**0.8825**	0.7583	0.5102

Testing Gas: 50% argon Result: 50% argon

Table 5-16 summarizes the results from table 5-1 to table 5-15 and shows that the database system can successfully recognize 20% oxygen, 30% oxygen, 40% oxygen, 10% helium, 10% argon, 40% argon, and 50% argon. The measurement for helium has a large deviation. However, even some recognitions for oxygen and argon failed, the deviations are not very large.

Table 5-16. The result table of all gases.

	10%	20%	30%	40%	50%
Oxygen	15% Helium	20% Oxygen	30% Oxygen	40% Oxygen	45% Oxygen
Helium	10% Helium	15% Oxygen	15% Argon	30% Oxygen	40% Oxygen
Argon	10% Argon	25% Argon	35% Argon	40% Argon	50% Argon

5.2 Result Analysis

The data obtained from the experiments exhibit a tendency of recognizing gases with their concentrations except for the recognition of helium. The reason for some gases to be unrecognized is probably the difficulty of the sensors offsets, i.e. the molecules of the gases are not able to be completely flushed from the surface of the polymer without vacuum condition. Moreover, polymers coated on the sensor will be looser and looser after a long operation of days, which result in signal drifts.

5.3 Recommendation for future works

In order to improve this research in future, five recommendations are suggested in this research. First, the frame design of the chamber needs to be enhanced so that a vacuum pump can be used to remove molecules on the surface of the polymer to acquire better signals. Second, the polymers selected need to be void of surfaces with viscous liquid phases. When the polymers are coated on the sensors, the properties of the polymers should be solid phase instead of viscous liquid phase. Third, sensors selected should be able to last longer, and have less drift and hysteresis so that the result may be consistent. Fourth, the equipment used should extend the database from 0% to 100%. Fifth, when establishing the database, a smaller scale between two concentrations is suggested to make precise recognitions.

REFERENCE

[1] Paul E. Keller "*Overview of Electronic Nose Algorithms*," IEEE conference, PP.309-312. 1999.

[2] http://www.hhmi.org/research/investigators/buck.html

[3] http://www.hhmi.org/research/investigators/buck_bio.html

[4] http://www.hhmi.org/research/investigators/axel_bio.html

[5] Claudia Di Nucci, Ada Fort, SantinaRocchi, Luca Tondi, Valerio Vignoli, Fabio Di Francesco, and M. Belen Serrano Santos "*A Measurement System for Odor Classification Based on the Dynamic Response of QCM Sensors*," IEEE Transection on Instruction and Meeasurement, Vol. 52, No. 4, August, 2003.

[6] M. Z. Atashbar, B. Bejcek, A. Vijh and S. Singamaneni "*Sensitivity Enhancement of a QCM Biosensor using Polymer Treatment*," IEEE Conference, PP.329-332, 2004.

[7] Jay. W. Grate "*Acoustic Wave Microsensor Arrays for Vapor Sensing*" Chem. Rev., PP. 2627-2648, 2000.

[8] Andreas Janshoff, Hans-Joachim Galla, and Claudia Steinem *"Piezoelectric Mass-Sensing Devices as Biosensors – An Alternative to Optical Biosensors?"* Angew.Chem. Int. Ed., 2000, 39, 4004-4032.

[9] Kenneth A. Marx *"Quartz Crystal Microbalance: A Useful Tool for Studying Thin Polymer Films and Complex Biomolecular Systems at ths Solution- Surface Interface,"* American Chemical Society, Vol.4, Number.5, PP.1099-1120, 2003.

[10] Richard P. Buck, Erno Lindner, Wlodzimierz Kutner and Gyorgy Inzelt *"Piezoelectric Chemical Sensors,"* Pure Appl. Chem, Vol. 76, No.6, PP. 1139-1106, 2004.

[11] K. Bizet, C. Gabrielli and H. Perrot *"Biosensors Based on Piezoelectric Transducers,"* Analusis, PP. 609-616, 1999.

[12] G. Sauerbrey *"Verwendung von Schwingquarzen zur Wägung dünner Schichten und zur Mikrowägung,"* Zeitschrift für Physik A Hadrons and Nuclei, Vol.155, Num.2, PP.206-222, 1959.

[13] Donald M. Candelaria "*Experimental Investgations on Gas Detection Using QCM Sensor Array and Phase-Locked Loop,*" MS Thesis.

[14] W. Patrick Carey, Kenneth R. Beebe, Bruce R. Kowalski, Deborah L. Illman and Tomas Hirschfeld "*Selection of Adsorbates for Chemical Sensor Array by Pattern Recognition,*" Anal. Chem., PP. 149-153, 1986.

[15] Jay W. Grate, Michael H. Abraham "*Solubility of Interactions and the Design of Chemically Selective Sorbent Coatings for Chemical Sensors and Arrays,*" Sensors and Actuators B, 3, PP. 85-111, 1991.

[16] Jay W. Grate and Steven N. Kaganove "*Comparisons of Polymer/Gas Partition Coefficients Calculated from Responses of Thickness Shear Mode and Surface Acoustic Wave Vapor Sensors,*" Anal. Chem., PP. 199-203, 1998.

[17] Abdolreza Mirmohseni and Vadood Hassanzaden *"Application of Polymer-Coated Quartz Crystal Microbalance (QCM) as a Sensor for BTEX Compounds Vapor,"* Journal of Applied Polymer Science, Vol. 79, PP. 1062-1066, 2001.

[18] Z. Ali, W. T. O' Hare, T. Sarkodie-Gyan and B. J. Theaker "*Gas-Sensing System Using An Array of Coated Quartz Crystal Microbalances with A Fuzzy Inference System,*" Journal of Thermal Analysis and Calorimetry, Vol. 55, PP. 371-381, 1999.

[19] Jay W. Grate, SamuelJ. Patrash, and Steven N. Kaganove *"Hydrogen Bond Acidic Polymers for Surface Acoustic Wave Vapor Sensors and Arrays,"* Anal. Chem., PP. 1033-1040, 1999.

[20] Jay W. Grate, Steven N. Kaganove and D. A. Nelson "*Polymers for Chemical Sensors Using Hydrosilylation Chemistry,*" PNNL-13556, 2001.

[21] Piyush Gupta, R. Thilagavathi, Asit K. Chakraborti, and Arvind K. Bansal "*Role of Molecular Interaction in Stability of Celecoxib – PVP Amorphous Systems,"* American Chemical Society, Molecular Pharmaceutics, Vol. 2, No. 5, PP. 384-391, 2005.

[22] Hanspeter Kahlig and Bernhard X. Mayer-Helm "*Characterization of Siloxane Copolymers by Solution 17ONMR Spectroscopy,*" Polymer 46, PP. 6447-6454, 2005.

[23] Guanrong Chen and Trung Tat Pham "*Introduction to Fuzzy Systems, 1st Edition,*" Chapman & Hall/CRC Applied, 2006.

[24] Didier Dubois and Henri Prade, "*Fuzzy Sets and Systems: Theory and Applications,*" Academic Press, Inc. 1980.

[25] L. A. Zadeh "*Fuzzy Sets,*" Information And Control 8, PP. 338-353, 1965.

[26] Magne Setnes, Robert Babuska, Uzay Kaymak, and Hans R. van Nauta Lemke, "*Similarity Measures in Fuzzy Rule Base Simplification,*" IEEE Transactions on Systems, MAN, and CYBERNETICS, Vol. 28, No. 3, June 1998.

[27] Roshdy S. Youssif and Carla N. Purdy, *"A Multistrategy Signal Pattern Classifier,"* IEEE Journal, Vol. 3 ,PP. III304-III307, 2002.

[28] Michael R. Jarrett and Harry O. Finklea, *"Detection of Nonpolar Vapors on Quartz Crystal Microbalances with* $Ni(SCN)_2(4-picoline)_4$ *Coatings,"* Anal. Chem., Vol. 71, No. 2, PP. 353-357, 1999.

[29] Harry O. Finklea, Mark A. Phillippi and Elisabeth Lompert, *"Highly Sorbent Films Derived from* $Ni(SCN)_2(4-picoline)_4$ *for the Detection of Chlorinated and Aromatic Hydrocarbons with Quartz Crystal Microbalance Sensors,"* Anal. Chem., Vol. 70, No. 7, PP. 1268-1276, 1998.

CURRICULUM VITA

Yi-Chen Lo was born in Pingtung, Taiwan. The first son of Ko-Lung Lo and Fang-Wei Tweng, He graduated from Pingtung Senior High School in June, 1998 and entered National Taiwan Ocean University, Keelung, Taiwan, in September 1999. In his pursuit of a Bachelor of Science degree, he majored in Mechanical-Electrical and Automation Control System in the department of System Engineering and Naval Architecture. After receiving his Bachelor of Science degree, he entered the army of Taiwan for 17 months of duty. He attended the University of Texas at El Paso in August, 2006, majoring in Electrical and Computer Engineering for pursuing his Master of Science degree. During his study in The University of Texas at El Paso, he obtained the Texas Instruments Foundation Endowed Scholarship in September, 2007, and worked as a teaching assistant for control systems, laboratory II, and computer-aided digital design. He received his Master of Science degree in December, 2008.

Permanent Address: No. 11-3, Fonghua St.

Pingtung 900, Taiwan